Journal of Engineering and Technology for Industrial Applications

ITEGAM-JETIA

Manaus, v.11 n.54, p. 205-214. July/August., 2025.
DOI: https://doi.org/10.5935/jetia. v11i54.1764

ISSN ONLINE: 2447-0228

RESEARCH ARTICLE OPEN ACCESS

ENHANCING THE COOLING SYSTEM DESIGN OF HIGH-POWER DENSITY PERMANENT MAGNET MOTOR FOR EV

Amit Kumar[1], Gaurav Singh Negi[2], Alok Sati[3]

[1, 2, 3] Uttaranchal Institute of technology, Uttaranchal University Dehradun India

[1]http://orcid.org/0009-0001-2643-3707, [2]http://orcid.org/0000-0003-1752-5359, [3]http://orcid.org/0009-0006-8591-761X

Email: akohli827@gmail.com technonegi@gmail.com, sati.alok9@gmail.com

ARTICLE INFO

Article History
Received: March 27, 2025
Revised: April 20, 2025
Accepted: June 15, 2025
Published: August 31, 2025

Keywords:
cooling system, PM motor, Taguchi Method Fluidic-thermal coupled analysis

ABSTRACT

Excessive losses inside permanent magnet (PM) motors in electric vehicle (EV) engine compartments can cause rapid temperature rises, deterioration of magnetic properties, limited output torques, and overheating. To ensure smooth operational condition, it's crucial to investigate and develop cost-effective cooling solutions for PM motors. This study presents a 3D fluidic-thermal linked model of a high-power density internal PM motor, based on Computational Fluid Dynamics and heat transfer theory. The fluid flow and heat dispensation are evaluated using the finite volume technique (FVM) and confirmed by practical results. Modifying the external fluid frame structure of the motor based on its heating properties improves cooling efficiency. The Taguchi approach improves cooling parameters to minimize the motor's temperature rise. This finding has significant implications for designing and developing high-power density Permanent motor for EV uses.

I. INTRODUCTION

The popularity and quick growth of electric vehicles (EVs) has led to substantial research into high-performance, reliable, and lightweight traction motors. The permanent magnet synchronous machine (PMSM) has great efficiency, power density, and power factor across various working circumstances. Permanent magnet motors are increasingly being used in electric vehicles (EVs) due to frequent start-stop and load changes in modern traffic. Excessive time harmonics from frequency converters in EV compartments can cause temperature rises, reduced magnetic density and coercivity, limited torque capacity, winding insulation damage, and irreversible PM demagnetization. Efforts to improve the power density of PM traction motors have been hindered by inefficient cooling systems [1]. External liquid cooling structures effectively cool machines and prevent leaks and erosion by avoiding direct contact between fluid flow and internal components (e.g. windings, cores, PMs) in EVs and HEVs. Cooling performance of a HEV four-quadrant transducer and found that changing the flow section profile increased heat dissipation. We investigated the impact of cooling medium and ratio on the temperature distribution of an EV traction motor using numerical calculations and actual measurements. We also tested the cooling performance of external liquid cooling frames outside the motor casing.

External cooling structures are commonly used in electric drive systems because to liquids' superior heat transfer capacity compared to gases. primarily due to high thermal resistance between the motor's end-windings, permanently magnets (PMs), and casings, which are in contact with the cooling frames [2]. In order to improve the heat dissipation, a new internal cooling system was developed by replacing the space in the motor where the cooling fluid would have to flow with fluid plates installed adjacent to the stator cores. The new internal cooling design enabled the stator core and windings to be directly cooled, with the internal cooling structure also having water tubes within the windings with direct water-cooling tubes on the stator core. The concept was tested on various PMSM high-power density prototypes. While the external cooling liquid extends in the motor cavity resulting in more cooling power, the cost of the prototype is significant. This research provides a 3D fluid structure interaction model for a new interior high-power density PM motor in electric vehicles (EVs). Numerical calculations based on FSI are used to calculate the flow state of the cooling medium and the distribution of

temperature rise in the motor. Calculations are confirmed by comparing them to experimental data. To increase heat dissipation for end-cap components, the liquid cooling design outside the motor case is optimized based on temperature rise distribution. The Taguchi approach is used to improvised cooling structure parameters, followed by numerical calculations and actual trials to determine temperature rise and optimal size [2,3].

II. MODEL AND SPECIFICATIONS

- **Structure and parameter**

a) The 20 kW, 4500 rpm PM motor has 4 pairs of permanent motor (PMs) and 48 slots. The circumference water frame is screw mounted on the outside of the motor casing to remove heat from the machine. The inside layout for the 20 kW 4500 rpm PM for EVs is shown in Fig. 1, where key specifications are shown in Table 1.[4]

b) **Assumptions and calculation**

To simplify the model and minimize calculation errors, the following assumptions are made for all motor parts involved in heat transmission.

Consider the model of motor's symmetry, Using the surrounding 1/8 model.

Table 1: High speed PMSM some parameters.

Quantity	Value
Max. speed	4500 rpm
Max. power	20kw
No. of pair of poles	4
Slots	48
Outer diameter Rotor core	125.6 mm
Outer diameter Stator core	194 mm
Air gap	0.7 mm
Axial length	75 mm
PM brand	N40UH
Soft iron sheet brand	35DW470
Liquid frame height	7.5 mm
Liquid frame width	20 mm

Source: Authors, (2025).

- The κ-ε mathematical framework employed to account for the high the ratio of inertial to viscous forces within a fluid of both the air confined in the end-caps and the liquid flowing in the liquid
- surround, caused by the rotor's air movement and the spiral channels' rapid water flow.
- Copper conductors are constructed from polymerized copper wires formed by wrapping them in insulating sheets. Furthermore, the conductors are made of wrapping insulation. Additionally, the insulation thickness is consistent across the copper conductor segment [5,6].
- Gaps are actually left unattended between the core of stator and the housing, and the rotor core and the permanent magnets.
- At the time of computations, they are represented as contact thermal resistances.
- Frictional loss is calculated taking into account internal air flow.

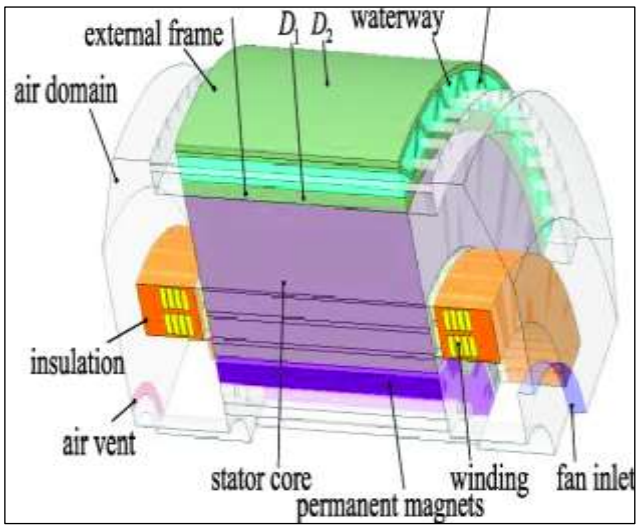

(a)

(b)

Figure 1: structure of permanent magnet motor a) basic model b) original model
Source: Authors, (2025).

The 3D Floor Space Index calculation model for the motor is created using basic assumptions and model simplifications, as seen in Figure 2. The model's outlet and inlet channels are lengthened to allow for turbulence before fluid enters spiral passages. The air's cross-section profiles are adjusted to periodic bounds to allow for passage through them [7].

III. THERMAL SOURCES

To get accurate distribution of the heat, it is tested for a complete load operation and then separated into losses in various components with all possible loss fraction is illustrated in Figure 3. The different loss components for the stator, rotor, and PMs have been calculated using finite element measurement while the frictional loss was found with the help of an empirical model [8].

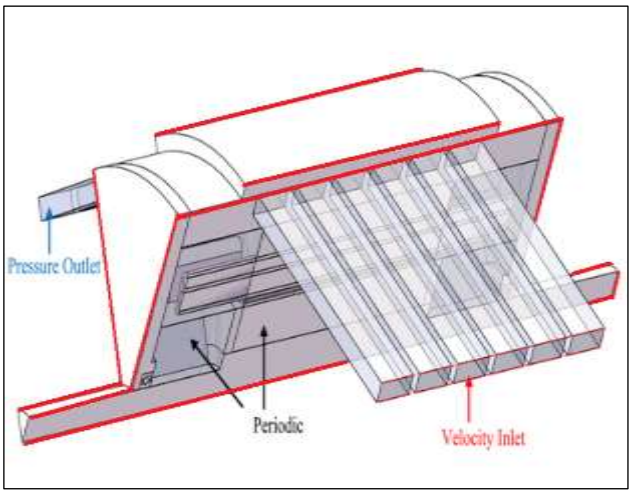

Figure 2: The structure of the PMSM with water barriers.
Source: Authors, (2025).

$$p\ (1)\ br = 0.772\ 5 \times 10^{-3} G_r\, D_{sh}\, n \qquad (1)$$

Gr (kg) = weight of rotor, Dsh (m) = shaft diameter, and n = rotational speed (rpm)Table 2 shows the heat production and losses rates.

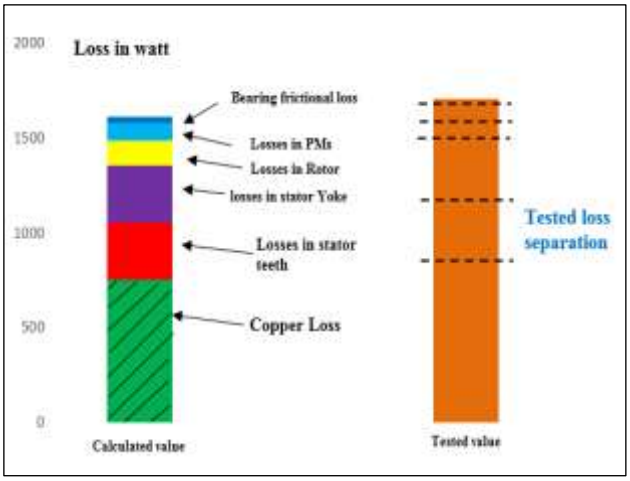

Figure 3: Losses and ratio.
Source: Authors, (2025).

- **Thermal analysis and consent**

The linked fluidic-heat areas are estimated using the calculation, frontier conditions, and motor thermal source dispensation. The central point of the PMs had the biggest temperature spike, measuring 134.7 K. Figure 4a displays the

Dispensation of temperature hike across the entire motor. Figure 4b displays the temperature hike of windings, with a peak value of 103.0 K. The figure shows that the end-windings experience a bigger temperature rise than the slots of windings due to the stronger heat transfer capacity of core of the stator compared to the convective air in the motor chamber [9]. Figure 4c displays the temperature rise distribution of permanent magnets, with a maximum value at 134.7 K. The heat from the rotor elements is partially dwindled by turbulent heat, corresponding to air in the gap traveling to the stator core in which conduction occurs to the water frames. Additionally, the shaft's conductive heat transfer capacity can serve as a heat dissipation conduit for rotor components. Heat transmission properties indicate that the middle region of PMs experiences a larger temperature rise compared to the end faces [10,11].

Table 2: Heat and losses measurement of machine.

Part	Loss in watt	Heat generation rate (x10^6 watt/m^3)
Rotor	99.50	0.267
Winding	758.50	3.523
Stator yoke	272	0.870
Stator teeth	339.60	0.785
Permanent magnets	89.06	1.507
Bearing	16.23	0.472

Source: Authors, (2025).

The experimental objectives are fixed to validate motor temperature rises. Wireless thermo sensors implanted in windings and affixed to the centre of the PMs measure heat rises in both. An infrared thermometer measures the temperature leap up of end-caps with the bearings [12]. Table 3 demonstrates how the mathematical findings are validated by comparing them to the experimental ones.

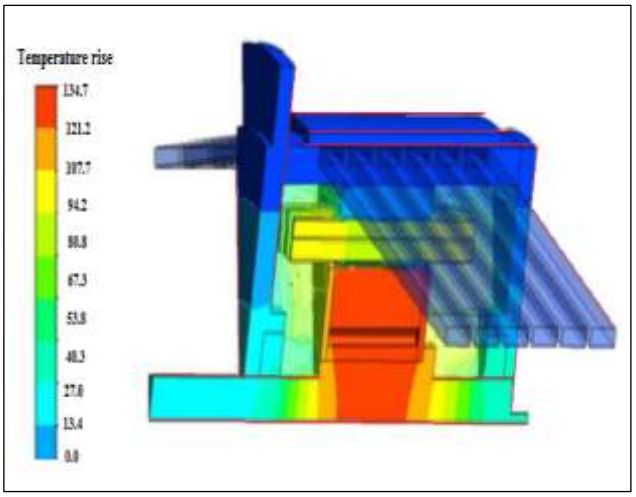

(a)

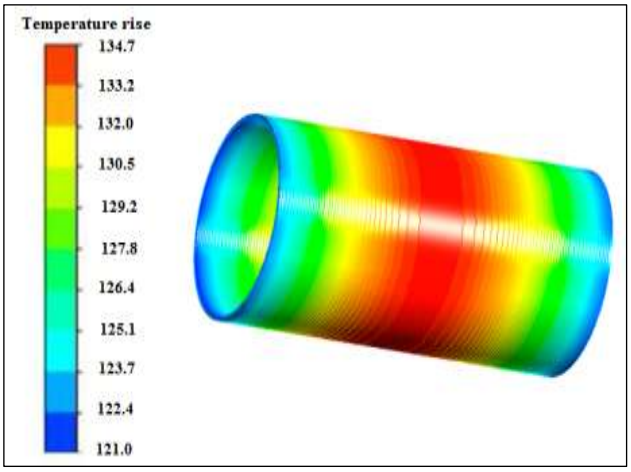

(b)

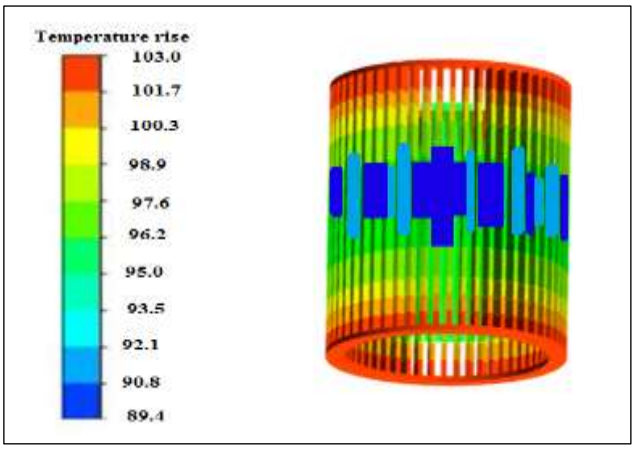

(c)

Figure 4: Temperature hike dissemination of PMSM with cooling structure a) motor b) winding c) permanent magnet.
Source: Authors, (2025).

IV. STRUCTURE OF COOLING MITIGATION

- **Structure of Cooling mitigation**

The computed temperature rises distributions indicate that the water-cooling frame's heat dissipation capacity on end-windings and PMs is restricted because of the high heating resistance between heating elements and liquid channels. To promote heat dissipation and reduce thermal resistance, an internal water channel structure is suggested (Figure 5) [13,14]

Table 3: temperature rise calculation of motor for water frame model.

Region	Calculation per 10^3	Testing per 10^3	Error %
winding	103.10	111.3	7.44 %
Permanent magnets	134.7	149.4	9.82 %
bearings	32.20	33.72	4.82

Source: Authors, (2025).

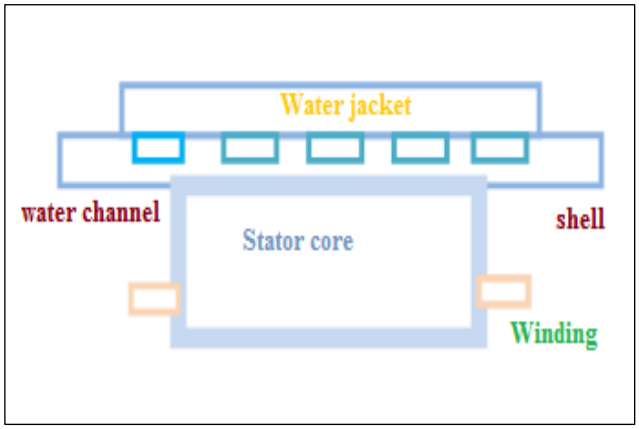

(a)

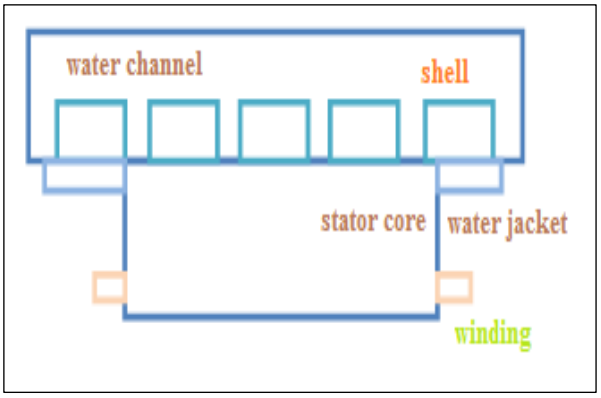

(b)

Figure 5: Improved fluid-cooled model of motor a) motor b) new model.
Source: Authors, (2025).

- **Structural Modification and Thermal Analysis of Motor**

Mathematical analysis is taken place on the liquid flow and temperature increase dissemination of a modified motor cooling structure. The largest temperature hike occurs in the canter region of the PMs at 128.3 K. The heat hike dissemination of the motor, as shown in Fig. 6, is comparable to that of the original construction (Fig. 4) [15,16,17]. The windings reached a maximum temperature of 97.3 K, which is 5.8 K less than the motor's main structure. The PMs have a maximum temperature rise of 128.3 K, which is 6.5 K much smaller the motor's main cooling arrangement. The redesigned water-cooling structure reduces winding temperature rise and indirectly improves rotor cooling capacity by reducing air temperature rise in end- caps [17, 18].

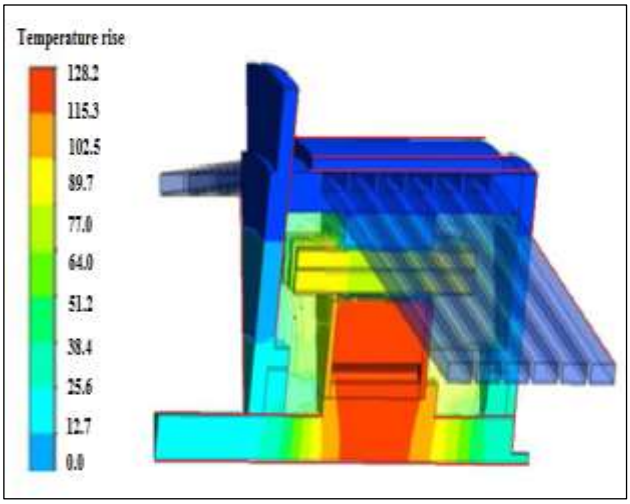

(a)

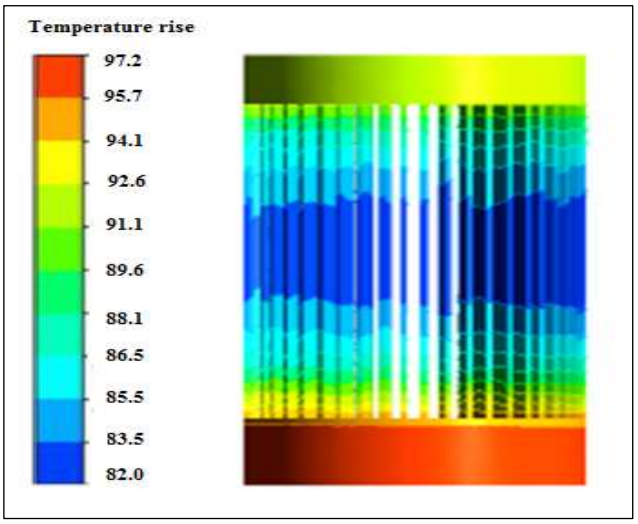

(b)

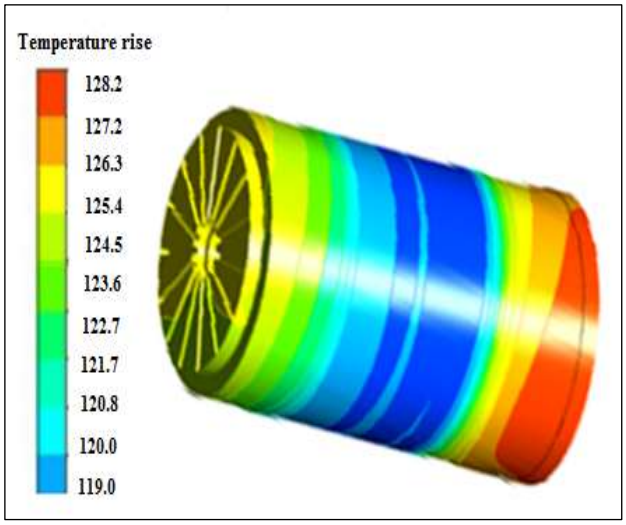

(c)

Figure 6: Temperature hike dissemination of PMSM with new cooling model a) motor b) winding c) permanent magnet.
Source: Authors, (2025).

V. ENHANCING THE REVISED COOLING

The Taguchi approach optimizes parameter combinations within a specific range with minimal experimental or computational effort. It is commonly employed in circumstances with high costs. Calculations for FSI problems can be time-consuming due to the fluidic-thermal coupled models' high level of nonlinearity [19,20]. The Taguchi approach is excellent for optimizing cooling structures. This work utilizes the Taguchi approach to the goal is to improved structural characteristics and increase heat dissipation capacity of a redesigned liquid frame cooling system. The parameters' sensitivity to heat dissipation performance is determined through analyses. The optimization processes consider the following factors: The circumferential channels are identified by their number (A), breadth (B), height (C), and fin width (D) [21, 22].

Table 4: Levels and factors.

Level	A	B	C	D
1	5	17.6	5.00	3.4
2	6	19.99	7.40	3.9
3	7	22.4	9.99	4.4

Source: Authors, (2025).

Table 5: L9(3^4) rectilinear and temperature rise.

Exp. No	A	B	C	D	Temperature rise per 10^3
1	2	2	2	2	128.2
2	2	1	1	1	125.4
3	2	3	3	3	129.8
4	1	2	1	3	127.2
5	1	1	3	2	130.3
6	1	3	2	1	128.4
7	3	2	3	1	130.6
8	3	1	2	3	128.5
9	3	3	1	2	124.6

Source: Authors, (2025).

Table 6. Average of each factor at various levels.

Factor	Level	Temperature rise per 10^3	Factor	Level	Temperature rise per 10^3
A	1	128.6	**C**	1	125.7
	2	127.8		2	128.4
	3	127.9		3	130.2
B	1	128.1	**D**	1	128.1
	2	128.6		2	127.7
	3	127.6		3	128.5

Source: Authors, (2025).

Table 4 shows the components and their related levels. Table 5 shows the use of the L9(34) orthogonal table due to the selection of four variables with three levels each. The cooling water flow rate (17.78 L/min) is maintained based on the factors table. Table 5 shows the maximal temperature rise of the PMs, which is likewise numerically determined [22,23,24]. Table 5 shows the temperature rise for

each group. Table 6 displays the general effect of each factor and level. The average temperature rise across 9 orthogonal experiments is calculated as:

$$T_{avg}\ \frac{\sum_{i=1}^{9} T_i}{9} = 128.2(\mathrm{K}) \tag{2}$$

Table 7: difference of every element with temperature hike.

Factor	A	B	C	D
S	0.12	0.16	3.41	0.10

Source: Authors, (2025).

Ti in (10^3) represents the temperature rise calculated. The error for every parameter can be calculated as follows:

$$S_j = \frac{\sum_{k=1}^{3} (T_{[3\mathrm{x(j-1)+k}]} - T_{ave})^2}{3} \tag{3}$$

Sj represents the square error of the jth factor. Table 7 shows square errors. Tables 6 and 7 indicate that:

- issue C (channel height) has a greater impact on temperature rise than other components, making it the primary issue to consider.
- By maintaining a stable cooling flow rate during optimization, reduced channel heights bring the cooling water to core, resulting in a greater cooling impact. Selecting level, I for factor C results in the lowest averaged temperature hike for the machine [25,26].
- Factor B (channel width) is second highest influence on heat hike. It is set to level III (22.5 mm) to greatly limit increase of temperature rise.

The effect of the variables A (no. of channel) and D (width) is minimal on motor temperature increment. Factor A is relevant to both the costs of manufacturing the cooling system as well as the output pressure of the pump. In order to lowest manufacturing, maintenance costs and operating for the cooling system factor A was set to level I (5 cycles). Factor D was set to II (4 mm) to result in the lowest average temperature hike [27,28,29].

The analysis finds the optimal parameters as A-I, b-III, C-I, and D-II. Temperature rise distributions of the motor using the optimal parameters are shown in Figure 7. The optimization process has reduced the temperature increase of the motor by 2.2 K, which indicates reliable operation of the PMSM for long term (see figures). To verify the results and ensure the enhance structure is efficient, a PMSM prototype was built based on the optimal structural parameters (Fig. 8) and tested for temperature rises. Table 8 compares temperatures rise calculated to those from testing [30].

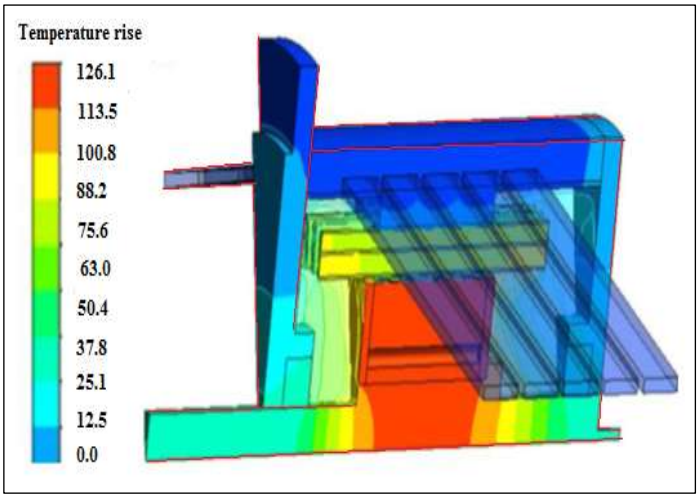

Figure 7: Temperature rise distribution of the motor with improvised cooling structure.
Source: Authors, (2025).

Figure 8: PM motor with improvised water-cooling structure.
Source: Authors, (2025).

Table 8: Calculation of Temperature hike and testing of the machine with new water model.

Parts	Calculation value per 1000	New value per 1000	Error
End winding	93.98	102.2	8.10 %
Permanent magnet	126.10	137.0	7.94 %
End cap (bearing)	29.7	30.6	2.92 %

Source: Authors, (2025).

VI. CONCLUSIONS

This study looks at the cooling efficacy of external water frames for a 20 kW 4500 rpm PM motor with high power density. Water channels are positioned on the inside surface of the motor housing to promote heat transfer. Numerical calculations support this approach. The Taguchi approach is used to optimize the formational characteristics of the enhanced cooling structure, thereby improving cooling performance. The study presented in this paper leads to the following findings:

- The three-dimensional thermal coupled approach is utilized to determine the temperature hike dispensation of the motor. The techniques' efficiency is demonstrated by the low calculation errors (< 10%) when compared to experimental results.
- Changing water channels from the external to interior exterior of the motor reduces the temperature rise by 6.5 K. Improving the cooling structure can improve heat dissipation in the cooling system.
- Optimization using the Taguchi approach improves cooling capacity and reduces temperature hike by 2.2 K.

VII. AUTHOR'S CONTRIBUTION

Conceptualization: Amit Kumar, Gaurav Singh Negi, Alok Sati.
Methodology: Amit Kumar, Gaurav Singh Negi, Alok Sati.
Investigation: Amit Kumar, Gaurav Singh Negi, Alok Sati.
Discussion of results: Amit Kumar, Gaurav Singh Negi, Alok Sati.
Writing – Original Draft: Amit Kumar, Gaurav Singh Negi, Alok Sati.
Writing – Review and Editing: Amit Kumar, Gaurav Singh Negi, Alok Sati.
Resources: Amit Kumar, Gaurav Singh Negi, Alok Sati.
Supervision: Amit Kumar, Gaurav Singh Negi, Alok Sati.
Approval of the final text: Amit Kumar, Gaurav Singh Negi, Alok Sati.

VII. ACKNOWLEDGMENTS

The authors would like to express their sincere gratitude to all those who contributed to the success of this research on enhancing the cooling system design of high-power density permanent magnet motors for electric vehicles (EVs). First and foremost, we would like to thank our research advisor, Gaurav singh negi, for their continuous guidance, support, and expertise throughout the course of this study. Their insightful comments and suggestions were invaluable in shaping the direction of this work.

We are also grateful to the members of the for their collaboration and technical support.

Finally, we would like to extend our heartfelt thanks to our families and friends for their patience, encouragement, and understanding during the course of this project.

VIII. REFERENCES

[1]. A. Morya, Applications of Wide Bandgap (WBG) devices in AC electric drives: a technology status review, in: 2017 IEEE International Electric Machines and Drives Conference (IEMDC), IEEE, 2017.

[2]. Park, J.-S.; Lee, T.-W.; Lee, J.-W.; Park, B.-G.; Kim, J.-W. Optimization of Multi-Phase Motor Drive System Design through Thermal Analysis and Experimental Validation of Heat Dissipation. Electronics 2023, 12, 4177.

[3]. Vlachou, V.I.; Sakkas, G.K.; Xintaropoulos, F.P.; Pechlivanidou, M.S.C.; Kefalas, T.D.; Tsili, M.A.; Kladas, A.G. Overview on Permanent Magnet Motor Trends and Developments. Energies 2024, 17, 538.

[4]. Dai, Y.; Wang, X.; Li, Z.; He, S.; Yu, B.; Zhou, X. Thermal error modeling of electric spindles based on cuckoo algorithm optimized Elman network. Int. J. Adv. Manuf. Technol. 2024, 132, 1365–1375.

[5]. Xiao, Y.; Zhu, Z.Q.; Jewell, G.W.; Chen, J.T.; Wu, D.; Gong, L.M. A Novel Asymmetric Interior Permanent Magnet Synchronous Machine. IEEE Trans. Ind. Appl. 2022, 58, 3370–3382.

[6]. H. Tahanian, M. Aliahmadi, J. Faiz, Ferrite permanent magnets in electrical machines: opportunities and challenges of a non-rare-earth alternative, IEEE Trans. Magn. 56 (3) (2020) 1–20.

[7]. E. Gundabattini, et al., A review on methods of finding losses and cooling methods to increase efficiency of electric machines, Ain Shams Eng. J. 12 (1) (2021) 497–505.

[8]. O. Wallscheid, et al., A critical review of techniques to determine the magnet temperature of permanent magnet synchronous motors under real-time conditions, EPE Journal 26 (1) (2016) 11–20.

[9]. Madhavan, S.; P B, R.D.; Gundabattini, E.; Mystkowski, A. Thermal Analysis and Heat Management Strategies for an Induction Motor, a Review. Energies 2022, 15, 8127.

[10]. Hu, X.; Yu, Z.; Zhuang, P.; Wan, J.; Wang, J.; Li, Y. Analytical Modeling of Temperature Field of SPMSM Based on Heat Pipe Cooling Technology. IEEE Trans. Appl. Supercond. 2024, 34, 5207705.

[11]. Liang, J.; Liang, K.; Shao, Z.; Niu, Y.; Song, X.; Sun, P.; Feng, J. Research on Temperature-Rise Characteristics of Motor Based on Simplified Lumped-Parameter Thermal Network Model. Energies 2024, 17, 4717.

[12]. A. Boglietti, A. Cavagnino, Analysis of the endwinding cooling effects in TEFC induction motors, in: Conference Record of the 2006 IEEE Industry Applications Conference Forty-First IAS Annual Meeting, IEEE, 2006.

[13]. G.M. Gilson, et al., A combined electromagnetic and thermal optimisation of an aerospace electric motor, in: The XIX International Conference on Electrical Machines-ICEM 2010, IEEE, 2010.

[14]. D.G. Nair, T. Jokinen, A. Arkkio, Coupled analytical and 3D numerical thermal analysis of a TEFC induction motor, in: 2015 18th International Conference on Electrical Machines and Systems (ICEMS), IEEE, 2015.

[15]. J. Park, et al., Design and analysis of high-speed permanent magnet motor considering thermal influence from impeller load characteristic of turbo blower system, in: 2016 IEEE Conference on Electromagnetic Field Computation (CEFC), IEEE, 2016.

[16]. N.K. Bhattacharya, D. Sarkar, Approximate analysis of transient heat conduction in the rotor of an induction motor during star-delta starting, in: International Conference on Information Communication and Embedded Systems (ICICES2014), IEEE, 2014.

[17]. Urbieta, J.G.; Rodríguez, B.; Rodríguez, A.J.; Díaz, P.; Armentia, S.; González, F. Sensitivity Analysis of Lumped-Parameter Thermal Networks for the Experimental Calibration of eMotor Models. IEEE Trans. Transp. Electrific. 2024, 10, 6210–6220.

[18]. Liu, Y.; Zhang, B.; Zong, M.; Feng, G. Thermal Analysis of a Modular Permanent Magnet Machine under Open-Circuit Fault with Asymmetric Temperature Distribution. Electronics 2023, 12, 1623.

[19]. IEC 60034-1; Rotating Electrical Machines—Part 1: Rating and Performance. International Electrotechnical Commission: Geneva, Switzerland, 2022.

[20]. Fasquelle, A.; Laloy, D. Water Cold Plates Cooling in a Permanent Magnet Synchronous Motor. IEEE Trans. Ind. Appl. 2017, 53, 4406–4413.

[21]. M. Jia, et al., Modeling and analysis of electromagnetic field and temperature field of permanent-magnet synchronous motor for automobiles, Electronics 10 (17) (2021) 2173.

[22]. B. Gan, et al., Thermal analysis of modular fault-tolerant permanent magnet motor based on electromagnetic-thermal Bi-directional coupling, IEEJ Trans. Electr. Electron. Eng. 17 (3) (2022) 454–469.

[23]. M. Jia, et al., Modelling and analysis of electromagnetic field and temperature field of permanent-magnet synchronous motor for automobiles, Electronics 10 (17) (2021) 2173.

[24]. C. Kim, K. Lee, Thermal nexus model for the thermal characteristic analysis of an open-type air-cooled induction motor, Appl. Therm. Eng. 112 (2017) 1108–1116.

[25]. G. Traxler-Samek, R. Zickermann, A. Schwery, Cooling airflow, losses, and temperatures in large air-cooled synchronous machines, IEEE Trans. Ind. Electron. 57 (1) (2009) 172–180.

[26]. G. Traxler-Samek, R. Zickermann, A. Schwery, Cooling airflow, losses, and temperatures in large air-cooled synchronous machines, IEEE Trans. Ind. Electron. 57 (1) (2009) 172–180.

[27]. Wang, L.; Shen, F.; Marignetti, F.; Bianchi, N.; Gong, H.; Li, Q.; Boglietti, A. Transient Thermal Exchange Analysis of an External Rotor Hub Motor for Electrified Defense Vehicles Applications Based on FVM and TNM. IEEE Trans. Transp. Electrific. 2024, 10, 1116–1127.

[28]. Wang, G.; Wang, Y.; Gao, Y.; Hua, W.; Ni, Q.; Zhang, H. Thermal Model Approach to the YASA Machine for In-Wheel Traction Applications. Energies 2022, 15, 5431.

[29]. Li, M.; Ye, J. Fractional Order Modeling of Thermal Circuits for an Integrated Energy System Based on Natural Transformation. Electronics 2022, 11, 914.

[30]. B. Gan, et al., Thermal analysis of modular fault-tolerant permanent magnet motor based on electromagnetic-thermal Bi-directional coupling, IEEJ Trans. Electr. Electron. Eng. 17 (3) (2022) 454–469.